ELSEVIER

Nuclear Instruments and Methods in Physics Research A 490 (2002) 614–629

NUCLEAR INSTRUMENTS & METHODS IN PHYSICS RESEARCH Section A

www.elsevier.com/locate/nima

Modeling quantum and structure noise of phosphors used in medical X-ray imaging detectors

N. Kalivas[a], L. Costaridou[a], I. Kandarakis[b], D. Cavouras[b], C.D. Nomicos[c], G. Panayiotakis[a,*]

[a] *Department of Medical Physics, School of Medicine, University of Patras, 26500 Patras, Greece*

[b] *Department of Medical Instrumentation Technology, Technological Educational Institution of Athens, Ag. Spyridonos Street, Aigaleo, Athens, Greece*

[c] *Department of Electronics, Technological Educational Institution of Athens, Ag. Spyridonos Street, Aigaleo, Athens, Greece*

Received 6 August 2001; received in revised form 13 March 2002; accepted 22 April 2002

Abstract

The noise properties of granular phosphors used in X-ray imaging detectors are studied in terms of a noise transfer function, NTF. This study is performed in high-exposure conditions where the contribution of structure noise to total screen noise is considerable. An analytical model, based on the cascaded linear systems methodology presented in the literature, is developed. This model takes into account the quantum noise and structure noise. Furthermore, it considers the effect of the K X-rays reabsorption on the phosphor material and the effect of screen thickness on the NTF. The model was validated against experimental results obtained by a set of Zn_2SiO_4:Mn phosphor screens prepared by sedimentation. The model may be used to evaluate the effect of screen thickness and the effect of the characteristic X-rays on NTF in high-exposure conditions where structure noise is considerable.

Keywords: Phosphor detector; Quantum noise; Structure noise; K X-rays; Model

1. Introduction

Phosphor materials, usually in the form of screens, are employed in the majority of medical X-ray imaging detectors. The intrinsic physical properties of these materials strongly affect image detector transfer characteristics, such as Modulation Transfer Function (MTF) and Noise Power Spectrum (NPS). Noise limits the quantity and quality of diagnostic information that an image detector can display [1,2]. In radiographic systems, either conventional (screen-film) or digital (e.g. phosphors coupled with CCD arrays), the total image noise is mainly due to the phosphor material noise (screen noise), as

*Corresponding author. Tel./fax: +30-610-996113.

E-mail address: panayiot@upatras.gr (G. Panayiotakis).

0168-9002/02/$ - see front matter
PII: S0168-9002(02)01088-4

well as the noise of various photodetectors (e.g. film, CCD) [2].Screen noise can be distinguished into two components, quantum and structure noises [2–6]. Quantum noise is attributed to the statistical nature of the spatial fluctuations of the absorbed X-ray quanta [4,8]. Quantum noise is the dominant noise component in low-exposure conditions, especially in the low and medium spatial frequency regions, i.e. below $20\,cm^{-1}$ [2,3,7]. For higher spatial frequencies and especially above $60\,cm^{-1}$ [2,3,5], quantum noise is comparable with the noise of film or CCD, since quantum noise decreases faster with spatial frequency [2]. Screen structure noise is attributed to fluctuations of the absorbed X-ray quanta due to the inhomogeneities in the phosphor coating [4]. This component is negligible in quantum-limited (i.e. low-exposure) conditions [4,5], but in higher exposure conditions it should be considered [2–4,6]. Screen noise is evaluated in terms of either NPS (also called Wiener spectrum), or Noise Transfer Function, NTF [7]. Since quantum and structure noise are statistically independent and uncorrelated [3–5,9], total screen NPS equals the sum of the corresponding NPS of quantum noise and screen-structure noise.

Published work on phosphor screen noise modeling considers either compact (e.g. CsI:Na) phosphor screens [10] or granular phosphors. In the case of granular phosphors, several quantum noise models have been developed [8,11,12]. In recent years, the use of cascaded linear systems methodology [13–15] has been incorporated into the study of signal and noise propagation in phosphor screens. This methodology has recently been enriched by considering the effect of the emission and reabsorbion of characteristic X-rays as well as the correlation between the sites of the characteristic X-rays emission and reabsorbtion [16,17]. The above work, however, does not take into account the effect of screen thickness or the X-ray photon energy spectrum. Furthermore, the quantum noise models that have been developed [7,18], by taking into account the effect of screen thickness, do not consider the characteristic X-rays. Recently, a model considering the effect of screen thickness as well as the characteristic X-rays on quantum noise has been developed [19], but without taking into account the effect of the correlation between the sites of the characteristic X-rays emission and reabsorption. [12,16,17]. Finally, all the aforementioned models treat noise in terms of quantum noise only, without considering structure noise.

In this study a granular phosphor screen NTF model, based on the cascaded linear systems methodology developed in the literature, for signal and noise propagation [13,14,16], is presented. The presented model considers both quantum and structure noises, the effect of K characteristic X-rays emission and reabsorption in the phosphor as well as the correlation between the sites of the characteristic X-rays emission and reabsorption. Finally, the thickness of the phosphor screen is also taken into account. The value of the presented model is validated against the experimental results obtained by a set of laboratory-prepared Zn_2SiO_4:Mn phosphor screens.

2. Materials and methods

2.1. Screen noise power spectrum

Let us assume a phosphor screen of thickness T with a corresponding surface density W. When an incident X-ray is absorbed in the phosphor material the signal in the output can be obtained by three different paths.

The first "path", path A, describes only the direct absorption of the incident X-rays without considering the presence of characteristic K X-rays. The third path, path C describes the absorption of the characteristic K X-rays. The intermediate path, path B corresponds to the X-ray energy given for the production of characteristic K X-rays minus the energy carried away by them. These paths may occur simultaneously (parallel) [16,17].

The total NPS, $NPS^{A+B+C}(u)$, where u is the spatial frequency, of the light signal is given by the following equation [16]:

$$\begin{aligned} NPS^{A+B+C}(u) = {} & NPS^{A}(u)+NPS^{B}(u)+NPS^{C}(u) \\ & + NPS^{AC}(u)+NPS^{AB}(u) + NPS^{BC}(u) \\ & + NPS^{BA}(u) + NPS^{CA}(u) + NPS^{CB}(u) \end{aligned} \quad (1)$$

where the first three terms correspond to the NPS of each process separately, while the next six terms are the cross-spectral density terms [16], which are zero in the case that the processes are statistically independent.

When an X-ray photon is absorbed without the production of characteristic K X-rays, the light photons escaping to the output are represented by process A. When an X-ray photon is absorbed with the production of K X-rays then processes B and C occur. However, it has been assumed that an X-ray photon will either be absorbed with process A or with processes B and C. Thus, processes A and B, as well as A and C, are statistically independent and their corresponding cross-spectral density terms are zero [16]. Therefore, $NPS^{AC}(u) = NPS^{AB}(u) = NPS^{BA}(u) = NPS^{CA}(u) = 0$. On the other hand, when an incident X-ray is absorbed and K X-rays are produced light is produced in the position where the incident X-ray is absorbed (path B), as well as in the positions where the characteristic K X-rays will be absorbed (path C). Thus, from a single interaction of an incident X-ray, where K X-rays are produced, there are two different paths of light photon generation and escape to the output, paths B and C. Therefore, the aforementioned paths are statistically correlated and their cross-covariances, or their equivalent in the spatial frequency domain cross-spectral density terms NPS^{BC} and NPS^{CB} are not zero[16].

Furthermore, $NPS^{BC}(u) = NPS^{CB}(u)$ [12,16]. By taking the above into account the total noise power spectrum if all the process are considered equals $NPS^{A+B+C}(u)_{q,s} = NPS^{A+B+C}(u)_q + NPS^{A+B+C}(u)_s$, where the indexes q and s refers to quantum noise power spectrum and structure noise power spectrum, where

$$NPS^{A+B+C}(u)_q = NPS^{A}(u)_{quantum} + NPS^{B}(u)_{quantum} + NPS^{C}(u)_{quantum} + 2NPS^{BC}(u) \quad (2a)$$

and

$$NPS^{A+B+C}(u)_s = NPS^{A}(u)_{structure} + NPS^{B}(u)_{structure} + NPS^{C}(u)_{structure}. \quad (2b)$$

Finally [7]

$$NTF^{2\,A+B+C}(u)_{q,s} = \frac{[NPS^{A+B+C}(u)_q + NPS^{A+B+C}(u)_s]}{[NPS^{A+B+C}(0)_q + NPS^{A+B+C}(0)_s]}. \quad (2c)$$

Each path is composed of a series of stochastic processes. These stochastic processes are considered to be the absorption of X-rays, the production of light quanta per absorbed X-ray, the escape of the light quanta to the output and the spread of the light quanta that have escaped to the output. These processes are distinguished into stochastic gain processes and blur processes. The general mathematical expressions that define the output NPS of each kind of process, if the input is known, are the following.

Let us consider, for example, a stochastic gain process. If $\bar{x}$ is the mean value of the input, $S_{xx}(u)$ is its NPS, where u is the spatial frequency, $\bar{A}$ is the mean "amplification" of the signal and var[A] is the variance of the amplification process, then the output NPS of the process, $S_{YY}(u)$ equals [13,14] $S_{YY}(u) = \bar{A}^2 S_{xx}(u) + \mathrm{var}[A]\bar{x}$ and the mean value of the output, $\bar{Y}$, equals $\bar{Y} = \bar{x}\bar{A}$.

Let us now consider the blur processes. These are characterized by an MTF(u) and they are distinguished into stochastic blur processes and deterministic blur processes [16,17]. For the case where $\bar{x}$ is the mean value of the input at a stochastic blur process and $S_{xx}(u)$ is the NPS of the input, the NPS of the output, $S_{ZZ}(u)$, equals [13,14] $S_{ZZ}(u) = [S_{xx}(u) - \bar{x}]\mathrm{MTF}^2(u) + \bar{x}$ and the mean value of the output, $\bar{Z}$ equals $\bar{x}$. Finally, if the process is a deterministic blur process, then the output NPS equals $S_{ZZ}(u) = S_{xx}(u)\mathrm{MTF}^2(u)$ and $\bar{Z}$ equals $\bar{x}$ [16,17].

In the case that there is more than one stage then each stage input is the output of the previous stage. The final output of each path can be obtained by cascading all the stages [13,14].

2.1.1. Modeling path A

Fig. 1 represents the aforementioned model for signal and noise propagation in the phosphor. It is assumed that the screen is divided into N thin layers of $M \times M$ pixels each [7,19–22]. Each layer is characterized by a mean surface density, $\overline{\Delta w}$, equal to W/N. The input of the system corresponds to the photon fluence of energy E, $f_n(E)$, incident on the nth layer. For this fluence, a power spectrum, $S^{A}_{nff}(E,u)$ and a mean fluence $\bar{f}_n(E)$ is considered, which accounts for the mean number of X-rays incident on the nth layer. Furthermore, $f_n(E)$ is considered as an uncorrelated Poison input, that is $S^{A}_{nff}(E,u) = \bar{f}_n(E)$ [13,14]. The first block describes the process of X-ray absorption of energy E in a pixel of the nth layer, $Q^{A}(E)$. This process is a stochastic gain process [7,13,14]. Considering all the pixels of the nth layer and many realizations of the process, a mean value $\bar{Q}^{A}(E)$ and a variance can be used to characterize this stage. This variance is considered to have two components: (i) A component already discussed in the literature [7,11,13] denoted in this work as $\mathrm{var}_q[Q^{A}(E)]$ and attributed to the stochastic process of X-ray absorption (i.e. quantum noise) and (ii) an additional component, accounting for the variations in $Q^{A}(E)$ due to the randomness of phosphor material deposition over the nth layer, proposed in this work. This component accounts for the structure noise and is denoted as $\mathrm{var}_s[Q^{A}(E)]$. Furthermore, we assume that these two components, of quantum and structure noise, are statistically uncorrellated; therefore, they can be added to yield the total variance of $Q^{A}(E)$. If $Q^{A}(E)$ is assumed to follow a binomial distribution with probability

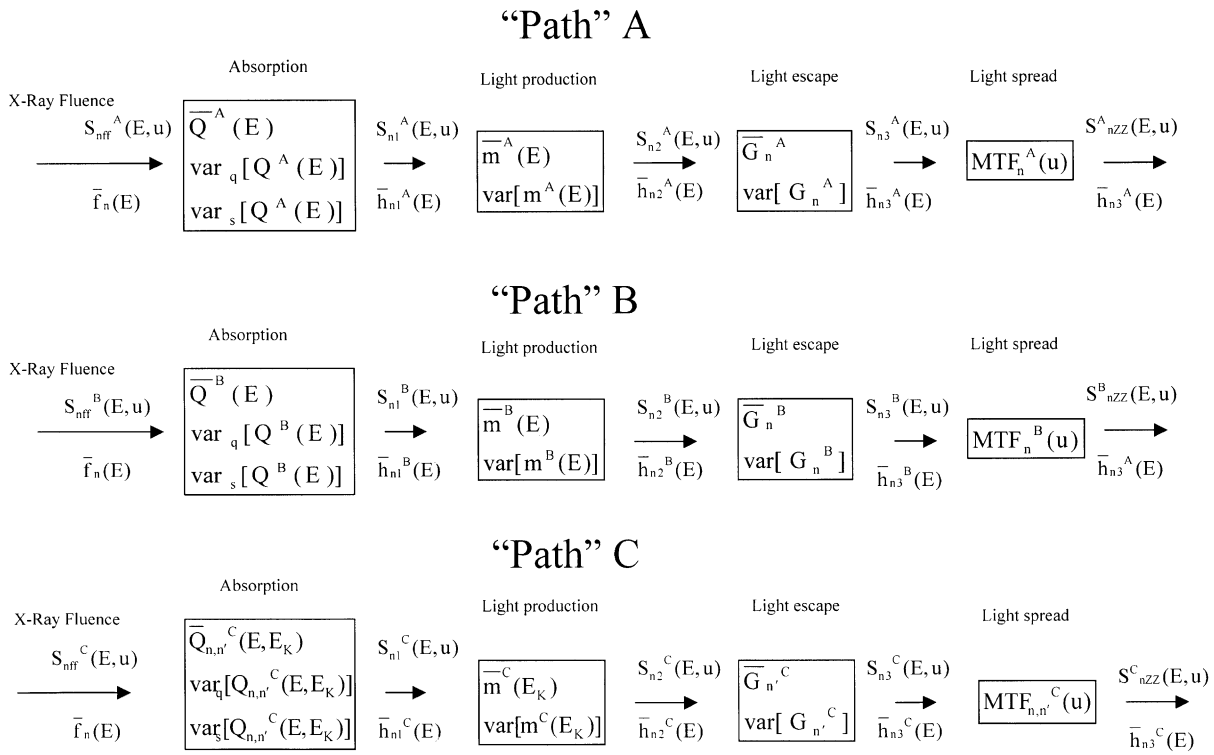

Fig. 1. Block diagram of the model.

$\bar{Q}^{A}(E)$ [11,13], then $\mathrm{var}_q[Q^{A}(E)] = \bar{Q}^{A}(E)(1-\bar{Q}^{A}(E))$. Finally, the output of this process is characterized by a corresponding mean value of the output signal denoted as $\bar{h}^{A}_{n1}(E)$ and a power spectrum denoted as $S^{A}_{n1}(E,u)$, where u is the spatial frequency.

The second block describes the light quanta generation in the phosphor at a pixel of the nth layer per absorbed X-ray of energy E, $m^{A}(E)$. This is also a stochastic gain process [7,13,14]. The second process depends upon inherent properties of the phosphor material regarding its capability in converting X-rays with energy E into optical photons. Therefore, it depends only upon the energy of the X-ray photon. Similarly, with the previous stage if all the pixels of the nth layer and many realizations of the process are considered, then a mean value, $\bar{m}^{A}(E)$ and a variance, $\mathrm{var}[m^{A}(E)]$, can be used to characterize this stage. The process of light generation per absorbed X-ray has been assumed to follow a Poisson distribution [2,7]; therefore, $\mathrm{var}[m^{A}(E)] = \bar{m}^{A}(E)$. However, even if the process is not Poisson, it has been shown that the effect of light production, gain and variations in NPS is comparable to a Poisson process [23] for the majority of granular phosphors. The output of this process is characterized by a corresponding mean value denoted as $\bar{h}^{A}_{n2}(E)$ and a power spectrum denoted as $S^{A}_{n2}(E,u)$.

The third block describes the process of light quanta, created at a pixel of the nth layer, escaping to the output, G^{A}_{n}. This stochastic gain process affects the optical photons generated in the second process; therefore, it does not depend upon the X-ray energy. If all the pixels and many realizations of the process are considered, then a mean value, $\bar{G}^{A}_{n}$, and a variance, $\mathrm{var}[G^{A}_{n}]$ can be used to characterize it. The process of light escape to the output is assumed to follow binomial distribution [7,11]. Thus, $\mathrm{var}[G^{A}_{n}] = \bar{G}^{A}_{n}(1-\bar{G}^{A}_{n})$. The output of the process is characterized by a corresponding mean value $\bar{h}^{A}_{n3}(E)$ and a power spectrum denoted as $S^{A}_{n3}(E,u)$.

The last block describes the spread of light quanta to the output. This is a stochastic blur process [7,13,14]. The effect of the last process is only a misplacement of the output of the light escape stage. The last process is characterized by a modulation transfer function $\mathrm{MTF}^{A}_{n}(u)$. The spreading stage is characterized by an output power spectrum denoted as $S^{A}_{nZZ}(E,u)$. The mean value of the spreading stage is the mean value of its input since the effect of this stage is only a misplacement of the input signal.

If the above stochastic processes are cascaded, by considering the general relations that define the output NPS of each process as described in Section 2.1, it is obtained that

$$\begin{aligned} S^{A}_{nZZ}(E,u) = {} & \bar{f}_n(E)\bar{Q}^{A}(E)[\bar{m}^{A}(E)\bar{G}^{A}_{n}\mathrm{MTF}^{A}_{n}(u)]^2 \\ & + \bar{f}_n(E)\bar{Q}^{A}(E)\bar{m}^{A}(E)\bar{G}^{A}_{n} \\ & + \{\bar{f}_n(E)\,\mathrm{var}_s[Q^{A}(E)]\}[\bar{m}^{A}(E)\bar{G}^{A}_{n}\mathrm{MTF}^{A}_{n}(u)]^2. \end{aligned} \tag{3a}$$

The above equation can be distinguished into three separate terms. The first two have already been introduced and discussed in the literature [7,13] and account for quantum noise power spectrum and the secondary quanta power spectrum. These are

$$\mathrm{NPS}^{A}_{n}(E,u)_{\mathrm{quantum}} = \bar{f}_n(E)\bar{Q}^{A}(E)[\bar{m}^{A}(E)\bar{G}^{A}_{n}\overline{\mathrm{MTF}}^{A}_{n}(u)]^2 \tag{3b}$$

and

$$W^{A}_{n,sq}(E) = \bar{f}_n(E)\bar{Q}^{A}(E)\bar{m}^{A}(E)\bar{G}^{A}_{n}. \tag{3c}$$

The third term, $\{\bar{f}_n(E)\mathrm{var}_s[Q^{A}(E)]\}[\bar{m}^{A}(E)\bar{G}^{A}_{n}\overline{\mathrm{MTF}}^{A}_{n}(u)]^2$, incorporates $\mathrm{var}_s[Q^{A}(E)]$, therefore can be considered to be related to structure noise. It will be called hereafter structure noise power spectrum, $\mathrm{NPS}^{A}_{n}(E,u)_{\mathrm{structure}}$:

$$\mathrm{NPS}^{A}_{n}(E,u)_{\mathrm{structure}} = \{\bar{f}_n(E)\mathrm{var}_s[Q^{A}(E)]\}[\bar{m}^{A}(E)\bar{G}^{A}_{n}\overline{\mathrm{MTF}^{A}_{n}}(u)]^2. \tag{3d}$$

2.1.1.1. Quantum noise. Equation (3b) gives the contribution of the nth layer to the total quantum noise for X-rays of energy E incident on the screen. If all the N screen layers are taken into account as well as an incident X-ray spectrum, quantum noise power spectrum equals

$$\mathrm{NPS}^{\mathrm{A}}(u)_{\mathrm{quantum}} = \sum_{E=0}^{E_{\max}} \sum_{n=1}^{N} \mathrm{NPS}_n^{\mathrm{A}}(E,u)_{\mathrm{quantum}} \tag{4}$$

where $E_{\max}$ is the maximum energy of the incident X-ray spectrum.

Assuming exponential attenuation of the beam in the phosphor the following analytical expressions can be used [7,18,22]:

$$\bar{f}_n(E) = \bar{f}(E)\mathrm{e}^{-\left[\mu_{\mathrm{tot}}(E)/\rho\right]n\overline{\Delta w}}$$

where μ_{tot}/ρ is the total linear mass attenuation coefficient for energy E and $\bar{f}(E)$ is the X-ray fluence incident on the phosphor screen. $\bar{Q}^{\mathrm{A}}(E)$ is the ratio of the X-rays absorbed over the X-rays incident on the nth layer, that is

$$\bar{Q}^{A}(E) = \frac{\bar{f}_n(E) - \bar{f}_n(E)\mathrm{e}^{-\left[\mu_{\mathrm{en}}(E)/\rho\right]\overline{\Delta w}}}{\bar{f}_n(E)} \quad \text{or} \quad \bar{Q}^{\mathrm{A}}(E) = 1 - \mathrm{e}^{-\left[\mu_{\mathrm{en}}(E)/\rho\right]\overline{\Delta w}}$$

where $\mu_{\mathrm{en}}(E)/\rho$ is the mass energy absorption coefficient. For the case where Δw is infinitesimally small, the equation calculating $\bar{Q}^{\mathrm{A}}(E)$ can be approximated by [19] $\bar{Q}^{\mathrm{A}}(E) = (\mu_{\mathrm{en}}(E)/\rho)\,\overline{\Delta w}$.

$$\bar{m}^{\mathrm{A}}(E) = n_{\mathrm{c}}\frac{E}{E_{\lambda}} \tag{5a}$$

where E_{λ} is the energy of the optical photons and n_{C} is the intrinsic conversion efficiency of the phosphor material [7,18].

A relationship for the product $\bar{G}_n^{\mathrm{A}}\mathrm{MTF}_n^{\mathrm{A}}(u)$ [7,24] is

$$\bar{G}_n^{\mathrm{A}}\mathrm{MTF}_n^{\mathrm{A}}(u) = \frac{\tau\rho_i[(b+\tau\rho_{\mathrm{o}})\mathrm{e}^{-bn\overline{\Delta w}} + (b-\tau\rho_{\mathrm{o}})\mathrm{e}^{-bn\overline{\Delta w}}]}{(b+\tau\rho_{\mathrm{o}})(b+\tau\rho_i)\mathrm{e}^{bW} - (b-\tau\rho_{\mathrm{o}})(b-\tau\rho_i)\mathrm{e}^{-bW}} \tag{5b}$$

where, b is an optical parameter given by $b = \sqrt{(\sigma^2 + 4\pi^2u^2)}$, σ is the reciprocal diffusion length, given by

$$\sigma = \sqrt{\alpha(\alpha+2s)} \tag{5c}$$

where a is the light photons absorption coefficient and s is the light photon scatter coefficient.τ is the inverse relaxation length given by $\tau = \sigma/\beta$. Additionally, τ can be expressed as a function of the a and s as

$$\tau = a + 2s. \tag{5d}$$

Both σ and τ characterize optical absorption and scattering, $\rho_i = (1-r_i)/(1+r_i)$, where r_i is the reflectivity of the inner surface of the screen at either the input, $i=0$, or the output, $i=1$, interfaces. Eq. 5(b) has been derived by Swank [23], under the following assumptions: (i) there are no discontinuities (in the sense of gross nonuniformities) in the properties of the screen, (ii) the probability of absorption is small compared with the probability of scattering and (iii) solutions are sought for points far from the source. Assumptions (i) and (ii) are valid for granular phosphors used in medical imaging [7,23]. Assumption (iii) is valid conditionally [7,19]. Furthermore, Eq. (5b) is for zero frequency given that $\mathrm{MTF}(0)=1$ gives $\bar{G}_n^{\mathrm{A}}$.

2.1.1.2. Structure noise. Eq. (3d) describes the $\mathrm{NPS}_n^{\mathrm{A}}(E,u)_{\mathrm{structure}}$. When the N layers of the phosphor screen as well as an incident polyenergetic X-ray spectrum is considered then the total screen structure NPS equals

$$\mathrm{NPS}^{\mathrm{A}}(u)_{\mathrm{structure}} = \sum_{E=0}^{E_{\max}} \sum_{n=1}^{N} \mathrm{NPS}_n^{\mathrm{A}}(E,u)_{\mathrm{structure}}. \tag{6}$$

In order Eq. (3d) and subsequently Eq. (6) to be evaluated $\mathrm{var}_s[Q^{\mathrm{A}}(E)]$ must be expressed. The fluctuations in $Q^{\mathrm{A}}(E)$ resulting in structure noise are attributed to changes in the elementary surface density Δw due to differences in the number of phosphor grains deposited. Assuming a random distribution of phosphor grains in each layer $\mathrm{var}_s[Q^{\mathrm{A}}(E)]$ can be calculated by means of its expected mean square error (Appendix A) as

$$\mathrm{var}_s[Q^{\mathrm{A}}(E)] = \left[\frac{\mu_{\mathrm{en}}(E)}{\rho}\right]^2 \left(\frac{\rho V_{\mathrm{g}}}{S}\right)^2 \zeta \frac{W}{N\rho V_{\mathrm{g}}} \tag{7}$$

where the parameters of Eq. (7) are defined in Appendix A.

2.2. Escape and absorption of characteristic X-rays

If the incident X-ray energy encompasses the K-edge of the phosphor material, then there are three possible sequence of events, "paths" [12,16]. The absorption of the X-ray photon energy at the interaction site without the production of a K X-ray photon, already described in path A. The absorption of the primary X-ray accompanied by the emission of K photons, referred in this text as path B. Finally, the K photons that are produced are absorbed in different locations within the phosphor material, referred in the text as path C.

2.2.1. Modeling path B

In Fig. 1 path B is also demonstrated. It is observed that the processes describing path B are the same as path A. The only difference related to path A occurs in the absorption process, first block, which describes the process of X-ray absorption in the nth layer accompanied by the production of K X-rays. This process refers to the fraction of the incident X-rays of energy E that were absorbed and yield K-photons, but without offering all of their energy to the production of K photons in the nth layer. Furthermore, all the assumptions regarding the mean values and variance that characterize each process are similar to path A.

Since path B is composed of the same type of processes as in path A, the equations describing it will be similar to Eqs. (3a)–(3d) of path A, as long as index A is replaced with index B.

2.2.1.1. Quantum noise. The quantum noise contribution of path B, if the N phosphor layers and the energy spectrum above K-edge are considered equals

$$\mathrm{NPS}^{\mathrm{B}}(u)_{\mathrm{quantumK}} = \sum_{E=E_{\mathrm{K}}}^{E_{\max}} \sum_{n=1}^{N} \mathrm{NPS}^{\mathrm{B}}_n(E,u)_{\mathrm{quantumK}} \tag{8}$$

where E_{K} is the K-edge energy.

An expression of $\bar{Q}^{\mathrm{B}}(E)$ can be found by considering that the X-ray photons absorbed at the nth layer and yield K photons do not offer all their energy to the production of characteristic photons [12].

$Q^{\mathrm{B}}(E)$ can be considered as the ratio of the remaining energy at the nth layer after the escape of K photons, $\bar{I}_n(\mathrm{E})$ to the energy of the X-rays incident at the nth layer $\bar{f}_n(E)E$. That is $\bar{Q}^{\mathrm{B}}(E) = \bar{I}_n(E)/\bar{f}_n(E)E$. When the incident X-rays, of energy E, interact in the nth layer then a total energy of $\bar{\Phi}_n(E)$ is absorbed in the layer, where $\bar{\Phi}_n(E) = \bar{f}_n(E)E - \bar{f}_n(E)E\mathrm{e}^{-(\mu_{\mathrm{tot}}/\rho)\overline{\Delta w}}$, where for the case Δw is infinitesimally small $\bar{\Phi}_n(E) = \bar{f}_n(E)E(\mu_{\mathrm{tot}}/\rho)\overline{\Delta w}$ Part of this energy is absorbed without the production of K photons. This energy equals $\bar{f}_n(E)E(\mu_{\mathrm{en}}/\rho)\overline{\Delta w}$. The energy the K-photons carry away is given by [20,25]

$$\overline{K_n}(E) = \bar{f}_n(E)\mu_{\mathrm{tot}}/\rho\,\overline{\Delta w}\omega_{\mathrm{K}}E_{\mathrm{K}}\frac{\mu_{\mathrm{pe}}/\rho}{\mu_{\mathrm{tot}}/\rho}o_{\mathrm{z}}f_{\mathrm{K}}I_{\mathrm{K}} \tag{9}$$

where ω_{K} is the fluorescence yield, E_{K} is the mean energy of K-characteristic photons of the phosphor, o_z is the fractional weight of the high Z element of the phosphor. μ_{pe}/ρ is the photoelectric mass attenuation

coefficient at energy E. f_K is the K-shell contribution to the photoelectric effect for the high Z element of the phosphor, I_K is the relative frequency of K-photons production [20,25].

After the escape of the K X-rays, the energy remaining in the nth layer, $\bar{I}_n(E)$ equals

$$\bar{I}_n(E) = \bar{f}_n(E)E\frac{\mu_{tot}}{\rho}\overline{\Delta w} - \bar{f}_n(E)E\frac{\mu_{en}}{\rho}\overline{\Delta w} - \bar{K}_n(E). \tag{10}$$

Therefore, $\bar{Q}^B(E)$ can be found by dividing Eq. (10) with $\bar{f}_n(E)E$, that is

$$\bar{Q}^B(E) = \frac{\mu_{tot}}{\rho}\overline{\Delta w} - \frac{\mu_{en}}{\rho}\overline{\Delta w} - \omega_K\frac{\mu_{pe}/\rho}{\mu_{tot}/\rho}o_z f_K I_K\frac{E_K}{E}\frac{\mu_{tot}}{\rho}\overline{\Delta w} \tag{11}$$

where $\overline{K_n}(E)$ has been substituted from Eq. (10). Furthermore, $\bar{m}^B(E)$ and $\bar{G}_n^B\mathrm{MTF}_n^B(u)$ are given by Eq. (5a) and (5b), respectively.

2.2.1.2. Structure noise. The corresponding equation of structure noise for path B, $\mathrm{NPS}^B(u)_{structure}$ if the N phosphor layers and the energy above K-edge is considered equals

$$\mathrm{NPS}^B(u)_{structure} = \sum_{E=E_K}^{E_{max}}\sum_{n=1}^{N}\mathrm{NPS}_n^B(E,u)_{structure}. \tag{12}$$

The value of $\mathrm{var}_s[Q^B(E)]$ is determined similar to path A. The corresponding value of $\mathrm{var}_s[Q^B(E)]$ is

$$\mathrm{var}_s[Q^B(E)] = \left(\frac{\mu_{tot}}{\rho} - \frac{\mu_{en}}{\rho} - \omega_K\frac{\mu_{pe}/\rho}{\mu_{tot}/\rho}w_z f_K I_K\frac{E_K}{E}\frac{\mu_{tot}}{\rho}\right)^2\left(\frac{\rho V_g}{S}\right)^2\zeta\frac{W}{N\rho V_g}. \tag{13}$$

2.2.2. Modeling path C

In Fig. 1 path C is demonstrated. It is observed that the processes describing path C are the same as that of paths A and B. The input of the system is the photon X-ray fluence, $f_n(E)$ incident on the nth layer. In the nth layer, K characteristic X-rays are produced. The first block describes the absorption of the K X-rays in the n'th layer, where $n' \neq n$. This process is denoted as $Q^C_{n,n'}(E, E_K)$, where E_K is the average energy of the K photons. The second and the third block describe the light production at the n'th layer per absorbed K X-rays and the light escape to the output, similar to the other "paths". The last block describes the spread of light quanta to the output. This process is characterized by a modulation transfer function which incorporates two procedures. The spread of the characteristic X-rays from the site of their production of the nth layer to the sites of their absorption on the n'th layer and the misplacement of the output of the light escape stage.

Furthermore, all the assumptions regarding the mean value and variance that characterize each process are similar to path A.

Since path C is composed of the same type of processes as in path A, the equations describing it will be similar to Eqs. (3a)–(3d) of path A, as long as index A is replaced with index C.

2.2.2.1. Quantum noise. If the phosphor screen N layers and the X-ray spectra above K-edge are considered, then $\mathrm{NPS}^C(u)_{quantum}$ equals

$$\mathrm{NPS}^C(u) = \sum_{E=E_K}^{E_{max}}\sum_{n=1}^{N}\sum_{n'=1}^{N}\mathrm{NPS}^C_{n,n'}(u,E)_{quantum} \tag{14}$$

where in Eq. (14) the summation is both over n and n'.

$\bar{Q}^C_{n,n'}(E, E_K)$ can be estimated as the ratio of the energy that the K X-rays, originating from the nth layer, have deposited to the n'th layer, $\bar{Y}_{n,n'}(E, E_K)$, to the total X-ray energy incident on the nth layer $\bar{f}_n(E)E$ or else $\bar{Q}^C_{n,n'}(E, E_K) = \bar{Y}_{n,n'}(E, E_K)/\bar{f}_n(E)E$.

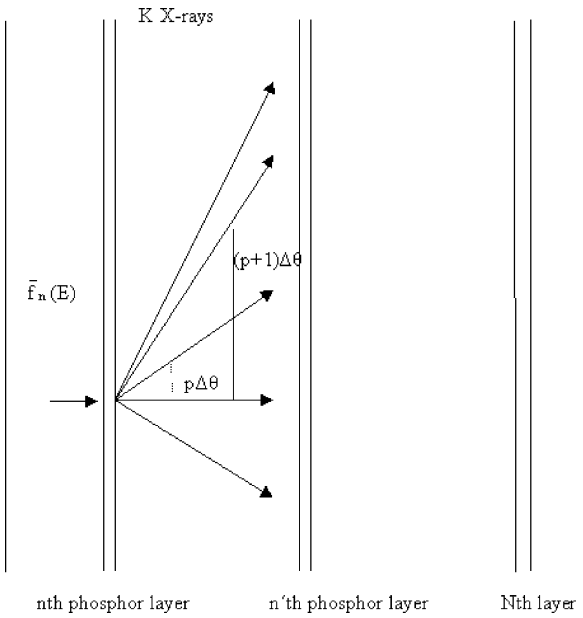

Fig. 2. A schematic representation of the K X-rays generation in an elementary layer Δw at position n and absorption within an elementary layer Δw at position n' of the phosphor.

Fig. 2 corresponds to a two-dimensional schematic representation of the K X-rays interactions within the phosphor screen. The produced K-characteristic photons have been assumed to be emitted isotropically, from the point of their creation within a solid angle 4π [20,25,26]. If the solid angle is divided into $2m$ solid angle elements denoted by $\Delta\Omega_p$ then

$$\Delta\Omega_p = 2\pi[\cos(p-1)\Delta\theta - \cos(p\Delta\theta)], \quad p = 1, 2, \ldots, 2m \tag{15}$$

where $\Delta\theta$ is the polar angle, which is equal to $\pi/2m$ [20]. Thus, the energy carried away by K photons per solid angle element equals $(\Delta\Omega_p/4\pi)\bar{K}_n(E)$. The K X-rays will interact in the screen and a part of their energy will be absorbed. K X-rays will interact at different layers. If the n'th layer of surface density Δw is considered, the K X-rays, originating from the nth layer, absorbed in it per solid angle element equals [19,26]

$$\bar{Y}_{p,n,n'}(E, E_K) = \bar{f}_{p,n,n'}(E, E_K)(1 - e^{-(\mu_{enK}/\rho)\overline{\Delta w}/\cos(p\Delta\theta)}), \quad n, n' = 1, 2, \ldots, N, n \neq n \tag{16a}$$

where

$$\bar{f}_{p,n,n'}(E, E_K) = \frac{\Delta\Omega_p}{4\pi E_K}\bar{K}_n(E)e^{-(\mu_{enK}/\rho)|n-n'|\overline{\Delta w}/\cos(p\Delta\theta)} \tag{16b}$$

is the number of the K X-rays, generated in the nth layer, that is incident on the n'th layer with solid angle $\Delta\Omega_p$. (μ_{enK}/ρ) is the total linear mass energy absorption coefficient of the phosphor for energy E_K. Considering $2m$ solid angle elements $\bar{Y}_{n,n'}(E, E_K) = \sum_{p=1}^{m} \bar{Y}_{p,n,n'}(E, E_K)$. $\bar{m}^C(E_K)$ is expressed by Eq. (5a).

The value of $MTF^C_{n,n'K}(u)$ can be written as $T_{nK}(u)MTF^C_{n'}(u)$, where $MTF^C_{n'}(u)$ considers the spread of the light quanta created at the n'th layer and escape to the output. $T_{nK}(u)$ is associated with the spread of the K X-rays from their production site and their absorption elsewhere. It is called by Metz [12] as the characteristic transfer function. A method for calculating $T_{nK}(u)$ is demonstrated in Appendix B. Furthermore, $\bar{G}^C_{n'}MTF^C_{n'}(u)$ can be expressed by Eq. (5b).

2.2.2.2. Structure noise. The structure noise contribution of path C, if the N phosphor layers and the energy spectrum above K-edge are considered equals

$$\mathrm{NPS}^{\mathrm{C}}(u)_{\mathrm{structure}} = \sum_{E=E_{\mathrm{K}}}^{E\max} \sum_{n=1}^{N} \sum_{n'=1}^{N} \mathrm{NPS}_{n}^{\mathrm{C}}(E,u)_{\mathrm{structure}}. \tag{17}$$

The value of $\mathrm{var}_s[Q_{n,n'}^{\mathrm{C}}(E,\mathring{A}_{\hat{\mathrm{E}}})]$ is determined via its mean square error similar to path A as

$$\mathrm{var}_s[Q_{n,n'}^{\mathrm{C}}(E,E_{\mathrm{K}})] = \left[\frac{\sum_{p=1}^{m}\dfrac{\Delta\Omega_p}{4\pi E_{\mathrm{K}}}\bar{K}_n(E)\mathrm{e}^{-(\mu_{\mathrm{enK}}/\rho)|n-n'|\overline{\Delta w}/\cos(p\Delta\theta)}\mathrm{e}^{-(\mu_{\mathrm{enK}}/\rho/\cos(p\Delta\theta))\overline{\Delta w}}(\mu_{\mathrm{enK}}/\rho)/\cos(p\Delta\theta)}{\bar{f}_n(E)E}\right]^2 \times \left(\frac{\rho V_{\mathrm{g}}}{S}\right)^2 \zeta\frac{W}{N\rho V_{\mathrm{g}}}. \tag{18}$$

2.2.3. Cross-spectral density terms

In order to evaluate the effect of the correlation between the sites of the characteristic X-rays emission and reabsorption [12,16] the cross-spectral density terms, $\mathrm{NPS}^{\mathrm{BC}}$ and $\mathrm{NPS}^{\mathrm{CB}}$, must be calculated. A generic expression for these terms has been derived by Cunningham [12,16]:

$$\mathrm{NPS}^{\mathrm{BC}}(u) = \mathrm{NPS}^{\mathrm{CB}}(u) = \bar{S}_{\mathrm{input}}(u)\bar{P}^{\mathrm{B}}\bar{P}^{\mathrm{C}}\mathrm{MTF}^{\mathrm{B}}(u)\mathrm{MTF}^{\mathrm{C}}(u)T_{\mathrm{K}}(u) \tag{19}$$

where S_{input} is the input signal. Furthermore, $\bar{P}^{\mathrm{B}}, \bar{P}^{\mathrm{C}}$ represent the product of the mean values of the stochastic "amplification" processes corresponding to path B and path C, respectively. If this work is considered then $\mathrm{NPS}_{n,n'}^{\mathrm{BC}}(u)$ is obtained by setting $\bar{S}_{\mathrm{input}}(u) = \bar{f}_n(E)$, $\bar{P}^{\mathrm{B}} = \bar{Q}^{\mathrm{B}}(E)\bar{m}^{\mathrm{B}}(E)\bar{G}_n^{\mathrm{B}}$, $\bar{P}^{\mathrm{C}} = \bar{Q}_{n,n'}^{\mathrm{C}}(E,E_{\mathrm{K}})\bar{m}^{\mathrm{C}}(E_{\mathrm{K}})\bar{G}_{n,n'}^{\mathrm{C}}$ and $\mathrm{MTF}^{\mathrm{B}}(u)\mathrm{MTF}^{\mathrm{C}}(u)T_{\mathrm{K}}(u) = \mathrm{MTF}_n^{\mathrm{B}}(u)\mathrm{MTF}_{n'}^{\mathrm{C}}(u)T_{n\mathrm{K}}(u)$.

If all the N phosphor layers, as well as the energy spectrum, are taken into account then

$$\mathrm{NPS}^{\mathrm{BC}}(u) = \sum_{E=E_{\mathrm{K}}}^{E\max} \sum_{n=1}^{N} \sum_{n'=1}^{N} \mathrm{NPS}_{n,n'}^{\mathrm{BC}}(E,u). \tag{20}$$

2.4. Validation

In order to validate the model, a set of Zn_2SiO_4:Mn screens was prepared by sedimentation on fused silica substrates [27]. The phosphor material was supplied in powder form with a grain size of 7 μm, by Derby Luminescent Ltd. The noise measurement was performed by bringing the phosphor screens in close contact with a single emulsion, Agfa MAMORAY MR3-II, film and by irradiating them with a mammography X-ray unit 30 kVp (Mo–Mo target tube), 50 mA s. The exposure incident on the screen surface for these conditions was 1.179 R. These exposure conditions were chosen for three reasons. First, the greater percentage of the incident X-ray spectrum [28] was above the K-edge of the high Z element of the phosphor material, Zn ($Z = 30$) with a K-edge at 9.66 keV [29]. Second, the exposure conditions were high enough to ensure that screen structure NPS would be a considerable, even dominant, noise source of phosphor screen noise [3,5]. Third, the effect of Compton scatter for the tube voltage of 30 kVp on Zn_2SiO_4:Mn was $<2\%$ as it can be found from the relevant attenuation and absorption coefficients published in the literature [29].

The irradiation geometry for the validation of the model comprised transmission mode measurements. The exposed films were scanned with a CCD scanner (Agfa Duoscan II) with a pixel size of about 26 μm and 8-bit scanning parameters. For the image noise analysis, a uniformly exposed area of 1000×1000 pixels was selected. The film recorded Noise Power Spectrum, $\mathrm{NPS}_{\mathrm{exper}}(D,u)_{\mathrm{total}}$, was evaluated as the

Fourier Transform of the autocorrelation function of the density fluctuations of the film [5,6,30–32], where D is the corresponding optical density of the film. $\mathrm{NPS}_{\mathrm{exper}}(D,u)_{\mathrm{total}}$ includes phosphor screen NPS, film NPS and the scanner NPS. Since all these noise sources are uncorrelated [2,3,5], $\mathrm{NPS}_{\mathrm{exper}}(D,u)_{\mathrm{total}}$ is the sum of the noise sources individual NPS. In order to isolate the screen NPS, that is quantum NPS and structure NPS, the film NPS and the scanner NPS were subtracted by $\mathrm{NPS}_{\mathrm{exper}}(D,u)_{\mathrm{total}}$. This was achieved by exposing the film to a homogeneous light source [5,19] until the same optical density as in the case of the irradiated screen film was achieved. The film was then digitized. The corresponding Wiener spectrum, which included film NPS and scanner NPS was calculated as described before and subtracted from the total.

The remaining NPS term was the phosphor screen NPS, $\mathrm{NPS}(u,D)_{q,s}$. If the values of the noise power spectra at the phosphor output $\mathrm{NPS}^{\mathrm{A+B+C}}(u)_q$ and $\mathrm{NPS}^{\mathrm{A+B+C}}(u)_s$ are known, then the corresponding values of film recorded quantum noise power spectrum and structure noise power spectrum equals [9]

$$\mathrm{NPS}^{\mathrm{A+B+C}}(D,u)_q = (\log_{10}\mathrm{e})^2 G^2(D)\frac{\mathrm{NPS}^{\mathrm{A+B+C}}(u)_q}{\mathrm{NPS}^{\mathrm{A+B+C}}(0)_q}\frac{1}{\eta I\bar{f}(E)}$$

and

$$\mathrm{NPS}^{\mathrm{A+B+C}}(D,u)_s = (\log_{10}\mathrm{e})^2 G^2(D)\mathrm{NPS}^{\mathrm{A+B+C}}(u)_s$$

where G(D) is the gamma of the film, η is the absorption efficiency of the screen [7,22], I is the Swank factor [32]. The corresponding film recorded NTF is given by Eq. (2c).

The M_{O} X-ray spectrum utilized was obtained by the published data [28]. The values of μ_{tot}/ρ, μ_{en}/ρ and μ_{pe}/ρ for the different energies, as well as, the values of $f_{\mathrm{K}} = 0.870$, $E_{\mathrm{K}} = 8.73\,\mathrm{keV}$, $\omega_{\mathrm{K}} = 0.45$ were obtained by the published data [29,33].

Finally, the values of the parameters used in Eqs. (5a) and (5b) were obtained from literature (i.e. $n_{\mathrm{C}} = 0.08$, $\beta = 0.03$, $\sigma = 38\,\mathrm{cm}^2/\mathrm{g}$) [34].

3. Results and discussion

Fig. 3 shows the experimental and predicted NTF data for two Zn_2SiO_4:Mn screens of 30 and 80 mg/cm^2, determined at 30 kVp with molybdenum spectrum X-rays. The correlation between these experimental data and the theoretical model is also demonstrated in Fig. 3. It is observed that for a thin screen of 30 mg/cm^2, the coincidence between measured and calculated values is poor. This occurs because thin screens do not fully comply with assumptions (i) and (ii) presented in Section 2.1.1.1, necessary to derive relations (5b). That is: (i) The thin screen may not be perfectly homogeneous (i.e. presents discontinuities), due to lower uniformity in the phosphor grain deposition. (ii) The distance between the point of light creation within the phosphor mass and the screen output may not be adequate for the majority of the phosphor layers in thin screens.

However, the correlation between experimental and predicted data of the 80 mg/cm^2 phosphor is better than the thin screen of 30 mg/cm^2. Any discrepancies between experimental and theoretical results for the 80 mg/cm^2 phosphor occur due to the low atomic number of the phosphor material. That is, the X-rays tend to be absorbed near the exit of the phosphor screen, opposite the X-ray tube. Therefore, some of the phosphor layers considered are near the screen output and contribute considerably to the produced signal at the screen output. Therefore, even thicker screens of low atomic number materials may not fully comply with assumption (ii) presented in the Materials and method section.

A point worth commenting is that, under identical irradiation conditions, thick screens exhibit lower noise transfer functions values than thicker ones. This may be explained by considering that NTF is expressed as the weighted sum of the squares of the thin layers MTFs, which decrease with increasing

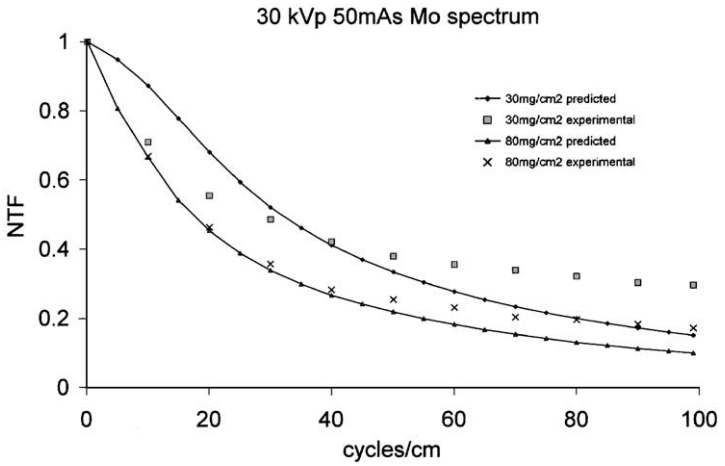

Fig. 3. Comparison between model-predicted and experimental NTF results for two Zn_2SiO_4:Mn phosphors, corresponding to coating thicknesses of 30 and 80 mg/cm^2.

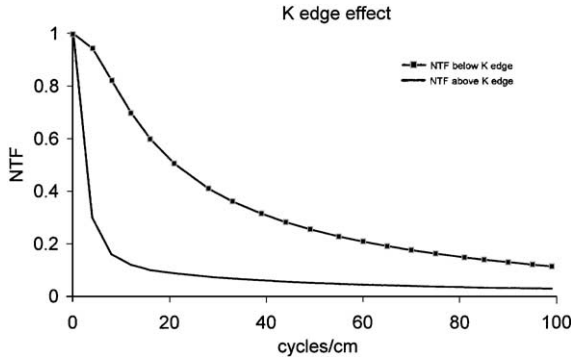

Fig. 4. Comparison of model-predicted NTF results just below and just above the K edge of the high Z element of the phosphor material, for a Zn_2SiO_4:Mn phosphor with surface density 80 mg/cm^2.

phosphor thickness, since the shape light bursts originating from depth t is broadened at thick phosphors [21]. Therefore, total screen NTF is decreased. However, total screen NTF decreases with screen and frequency is slower than the corresponding MTF decrease, since the latter is expressed as the weight sum of the MTFs of each thin layer [7,8,14].

Fig. 4 demonstrates a comparison of phosphor screen NTF just above and just below the K-edge. It is clearly observed that the NTF just above the K-edge is poorer than the NTF just below the K-edge. This occurs because the presence of K X-rays reduces the transfer characteristic of the phosphor screen, since a fraction of the energy carried away by the K X-rays is reabsorbed in sites away from the site of the primary interaction [32,35]. This in turn reduces total screen NTF. Furthermore, above the K-edge the absorption efficiency of the phosphor is highly increased, related to the absorption efficiency just below the K-edge. This has the consequence that the light photons are generated in layers near the input of the phosphor, thus their corresponding shape light bursts as the output is broadened. On the other hand, just below the K-edge there are no K X-rays and the absorption efficiency of the phosphor is reduced. Therefore, the interactions

mainly occur in layers near the screen output leading to a narrower shape of the light bursts and, therefore, better transfer characteristics [21] and higher NTF values.

Finally, it should be noticed that the experimental setup of this work considers mainly the effect of screen thickness in high-exposure conditions, where the screen structure noise is dominant, [3,5,6], in the presence of characteristic K X-rays. However, this model can be used for lower X-ray exposures. Specifically, it has been shown in the literature [3] that structure noise may be of importance, for phosphor X-ray detectors used in medical imaging, in cases where the number of absorbed X-ray photons in the phosphor screen exceeds 7000 photons/mm^2. The absorption efficiency of these phosphors is almost always over 20% in the energy range under consideration [39–40]. Therefore, structure noise could be under consideration if a number of X-ray photons is $>35\,000\,\mathrm{mm}^{-2}$, which is translated into exposures values below 1 mR [41,42], is incident on the phosphor screen surface.

Future efforts will include more X-ray energy spectra and grain sizes, as the latter seems to have a significant impact on structure noise according to our model. Specifically, if the grain size is increased to 12 μm leading to 3.6×10^6 phosphor grains/mm^2, the model predicts an increase in structure mottle to about five times. This behavior is expected, if one considers that the bigger the size of the phosphor grains the less uniformly they would be deposited. That is the macroscopic uniformity of the screen would be reduced.

4. Summary

This study presents an analytical NTF model which takes into account the K X-rays reabsorption in the phosphor screen in exposure conditions where the structure noise is considerable. The model shows good agreement with NTF experimental results of ZnSiO4:Mn phosphors irradiated with high-exposure conditions. Furthermore, the model describes in a satisfactory way the effect of screen thickness as well as the effect of the K characteristic X-rays on NTF for these exposure conditions.

Appendix A

A random value of $Q^{\mathrm{A}}(E)$ in an arbitrary pixel can be found as $Q^{\mathrm{A}}(E)=\mu_{\mathrm{en}}(E)/\rho\Delta w$. A way to calculate the variance of $Q^{\mathrm{A}}(E)$ is by means of its expected mean-square error [36,37], which is calculated in terms of the parameters mean values [37]:

$$\mathrm{var}_s[Q^{\mathrm{A}}(E)]\cong\left[\frac{\partial Q_n^{\mathrm{A}}(E)}{\partial\Delta w}\right]^2\mathrm{var}[\Delta w]. \tag{A.1}$$

By applying Eq. (A.1) to $Q^{\mathrm{A}}(E)$ one obtains

$$\mathrm{var}_s[Q^{\mathrm{A}}(E)]=\left[\frac{\mu_{\mathrm{en}}(E)}{\rho}\right]^2\mathrm{var}[\Delta w]. \tag{A.2}$$

The fluctuations in $Q^{\mathrm{A}}(E)$ resulting in structure noise are attributed to changes in the elementary surface density $\Delta w=\Delta m/S_{\mathrm{elementary}}$ due to differences in the phosphor mass, Δm, per elementary area $S_{\mathrm{elementary}}$ of the nth phosphor layer. If ρ is the phosphor material density and V is the volume of a phosphor grain, then $\Delta m=\rho V_{\mathrm{g}}L_{\mathrm{g}}$, where L_{g} is the number of phosphor grains deposited on $S_{\mathrm{elementary}}$ at the nth layer. The value of L_{g} may vary resulting in variations of Δw. If the phosphor grain is assumed to be spherical [38] then $V_{\mathrm{g}}=4/3\pi R_{\mathrm{g}}^3$ where R_{g} is the grain radius. Therefore, $\Delta w=\rho V_g/SL_g$ and

$$\mathrm{var}[\Delta w]=\left(\frac{\rho V_{\mathrm{g}}}{S}\right)^2\mathrm{var}[L_{\mathrm{g}}] \tag{A.3}$$

where [4]

$$\mathrm{var}[L_g] = \zeta \bar{L}_g \tag{A.4}$$

where ζ is an index of crowding and takes into account the constrain on Poisson randomness associated with the finite size and crowding of phosphor particles. It takes values ranging from 1 (no crowding) to 0 (complete crowding and macroscopic uniformity) [4]. The value of ζ can be obtained by the formula $\zeta = \delta^2/[\delta^2 + (2R_g)^2]$ [4], where $\delta = 2R_g\,[(74/55)^{1/3} - 2R_g]$. For a phosphor grain diameter, $2R_g$, of 7 μm, the value of ζ equals 0.0083.

The number of phosphor grains per layer per elementary area can be found as follows. Let us consider a phosphor screen of surface density W assumed to be divided into N thin elementary layers. To this phosphor screen corresponds a mass of phosphor material $M_{\mathrm{ph},}$ deposited over an area S_{total}. If the deposition process introduces no deterministic errors in the phosphor grain deposition, then it is assumed that the phosphor mass is uniformly distributed into the N layers; therefore, the expected phosphor mass per layer equals M/N. To this phosphor mass corresponds a number of phosphor grains which equals $M/(N\rho V_g)$. If this number of grains is divided with S_{total} then the number of phosphor grains per unit area is obtained, that is $\bar{L}_g = M/N\rho V_g S_{\mathrm{total}}$. Since by definition $W = M/S_{\mathrm{total}}$ it is obtained that $\bar{L}_g = W/N\rho V_g$. For a grain size of 7 μm diameter, a phopshor density of 3 g/cm^3 and a ratio W/N equal to 0.001 g/cm^2, a number of 1.9×10^7/mm^2 phosphor grains is expected.Finally,

$$\mathrm{var}_s[Q^{\mathrm{A}}(E)] = \left[\frac{\mu_{\mathrm{en}}(E)}{\rho}\right]^2 \left(\frac{\rho V_g}{S}\right)^2 \zeta \frac{W}{N\rho V_g}. \tag{A.5}$$

Appendix B

The spread of the characteristic X-rays, assuming that the escape and reabsorption of K X-rays is rotationally symmetric, can generally be expressed in the frequency domain as [12]: $2\pi \int_o^\infty \mathrm{CSF}(R) J_o(2\pi u R) R\,\mathrm{d}R$, where $J_o(2\pi uR)$ is the zero-order Bessel function [36]. $2\pi R\mathrm{CSF}(R)\Delta R$ expresses the probability that a K X-ray will be reabsorbed in the screen at a distance between R and $R + \Delta R$ (perpendicular to the direction of the incident X-rays) from the site of its production.

Fig. 5 is a two-dimensional representation of the K X-rays interaction in the phosphor, where R is indicated. If the $M \times M$ pixels of the layer are considered and assuming that ΔR is the size of the pixel at the direction of R then $R = i\Delta R$ where $i = 1, \ldots, M/2$. $2\pi R\mathrm{CSF}(i\Delta R)\Delta R$ can be calculated as follows.

Let us assume that the K X-rays are produced in the nth layer at the center of the area of the $M \times M$ pixels. As it is seen from Fig. 5 the number of K X-rays emerging from the nth layer, with a solid angle $\Delta\Omega_p$ and are incident at the n'th layer at a distance $R = i\Delta R$ were perpendicular to the direction of the incident X-rays equal to $\bar{f}_n(E)(\Delta\Omega_p/4\pi E_{\mathrm{K}})\bar{K}_n(E)e^{-((\mu_{\mathrm{enK}}/\rho)\rho i\Delta R)/\sin(p\Delta\theta)}$. Assuming exponential attenuation of the K X-rays, the number of the K X-rays absorbed at a distance between $i\Delta R$ and $i\Delta R + \Delta R$ perpendicular to the incident X-rays will be equal to

$$\bar{f}_n(E)\frac{\Delta\Omega_p}{4\pi E_{\mathrm{K}}}\bar{K}_n(E)\mathrm{e}^{-((\mu_{\mathrm{enK}}/\rho)\rho i\Delta R)/\sin(p\Delta\theta)} - \bar{f}_n(E)\frac{\Delta\Omega_p}{4\pi E_{\mathrm{K}}}\bar{K}_n(E)\mathrm{e}^{-((\mu_{\mathrm{enK}}/\rho)\rho(iR+\Delta R))/\sin(p\Delta\theta)}. \tag{B.1}$$

Therefore, the number of the K X-rays produced in the nth layer and absorbed in a distance between $i\Delta R$ and $i\Delta R + \Delta R$ can be found as

$$\sum_{p\Delta\theta=\theta_{\min}}^{2m} \bar{f}_n(E)\frac{\Delta\Omega_p}{4\pi E_{\mathrm{K}}}\bar{K}_n(E)\mathrm{e}^{-((\mu_{\mathrm{enK}}/\rho)\rho i\Delta R)/\sin(p\Delta\theta)} - \bar{f}_n(E)\frac{\Delta\Omega_p}{4\pi E_{\mathrm{K}}}\bar{K}_n(E)\mathrm{e}^{-((\mu_{\mathrm{enK}}/\rho)\rho(i\Delta R+\Delta R))/\sin(p\Delta\theta)} \tag{B.2}$$

where for a given distance R and according to Fig. 5, $\theta_{\min} = \arctan(i/N - n)$.

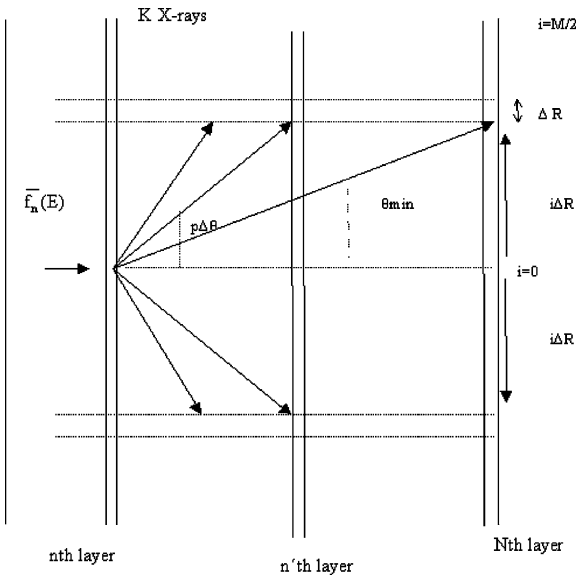

Fig. 5. A schematic representation of the K X-rays interactions within the phosphor where their absorption site perpendicular to the direction of the incident X-rays is indicated.

Furthermore, the number of K X-rays incident on $i\Delta R$ equals

$$\sum_{p\Delta\theta=\theta_{\min}}^{2m} \bar{f}_n(E)\frac{\Delta\Omega_p}{4\pi E_K}\bar{K}_n(E)e^{-((\mu_{enK}/\rho)\rho i\Delta R)/\sin(p\Delta\theta)}. \tag{B.3}$$

Therefore, $2\pi R\mathrm{CSF}(i\Delta R)\Delta R$ can be calculated as

$$2\pi R\mathrm{CSF}(i\Delta R)\Delta R = \frac{\sum_{p\Delta\theta=\theta_{\min}}^{2m} \bar{f}_n(E)\frac{\Delta\Omega_p}{4\pi E_K}\bar{K}_n(E)e^{-((\mu_{enK}/\rho)\rho i\Delta R)/\sin(p\Delta\theta)} - \bar{f}_n(E)\Delta\Omega_p/4\pi E_K\bar{K}_n(E)e^{-((\mu_{enK}/\rho)\rho(i\Delta R+\Delta R))/\sin(p\Delta\theta)}}{\sum_{p\Delta\theta=\theta_{\min}}^{2m} \bar{f}_n(E)\frac{\Delta\Omega_p}{4\pi E_K}\bar{K}_n(E)e^{-((\mu_{enK}/\rho)\rho i\Delta R)/\sin(p\Delta\theta)}}$$

Finally, the characteristic transfer function can be found as

$$T_{n\mathrm{K}}(u) = \frac{2\pi\sum_{i=0}^{M/2}\mathrm{CSF}(i\Delta R)J_o(2\pi ui\Delta R)i\Delta R\Delta R}{2\pi\sum_{i=0}^{M/2}\mathrm{CSF}(i\Delta R)J_o(2\pi 0i\Delta R)i\Delta R\Delta R}. \tag{B.4}$$

References

[1] R.S. Holland, in: A.G. Haus (Ed.), The Physics of Medical Imaging: Recording System, Measurements and Techniques, American Association of Physicists in Medicine, New York, 1979, pp. 152–171.
[2] R.M. Nishikawa, M.. Yaff, Med. Phys. 17 (1990) 887.
[3] H. Arimura, et al., J. Photogr. Sci. 40 (1992) 6.
[4] G.T. Barnes, Med. Phys. 9 (1982) 656.
[5] P.C. Bunch, K.E. Huff, R. Van Meter, J. Opt. Soc. Am. A 4 (1987) 902.
[6] W. Hillen, U. Schiebel, T. Zaengel, Med. Phys. 14 (1987) 744.

[7] R.M. Nishikawa, R. Yaffe, Med. Phys. 17 (1990) 894.
[8] G. Lubberts, J. Opt. Soc. Am 58 (1968) 1475.
[9] H. Arimura, et al., Phys. Med. Biol. 44 (1999) 1337.
[10] W. Hillen, W. Eckenbach, P. Quadflieg, T. Zaenkel, Proc. SPIE 1443 (1991) 120.
[11] R. Shaw, R. Van Meter, Proc. SPIE 454 (1984) 128.
[12] C.E. Metz, C.J. Vyborny, Phys. Med. Biol. 28 (1983) 547.
[13] M. Rabbani, R. Shaw, R. Van Meter, J. Opt. Soc. Am A 4 (1987) 895.
[14] R. Van Meter, M. Rabbani, Med. Phys. 17 (1990) 65.
[15] I.A. Cunningham, et al., Med. Phys. 21 (1994) 417.
[16] I.A. Cunningham, Proc. SPIE 3336 (1998) 220.
[17] I.A. Cunningham, et al., J. Opt. Soc. Am A 16 (1999) 621.
[18] I. Kandarakis, et al., Phys. Med. Biol. 42 (1997) 1351.
[19] N. Kalivas, et al., Nucl. Instr. and Meth. A 430 (1999) 559.
[20] H.-P. Chan, K. Doi, Phys. Med. Biol. 28 (1983) 565.
[21] R.M. Nishikawa, M. Yaffe, R.B. Holmes, Med. Phys. 16 (1989) 773.
[22] D. Cavouras, et al., Med. Phys. 23 (1996) 1965.
[23] N. Kalivas, et al., Appl. Phys. A 69 (1999) 337.
[24] R.K. Swank, Appl. Opt. 12 (1973) 1865.
[25] K.L. Yip, et al., Med. Phys. 23 (1996) 1727.
[26] D. McLean, J.E. Gray, Med. Phys. 23 (1996) 1253.
[27] G. Panayiotakis, et al., Appl. Phys. A 62 (1996) 483.
[28] R. Birch, M. Marshal, G.M. Asdran, Catalogue of Spectral Data for Diagnostic X-rays, HPA Scientific Report Series 30, Hospital Physicists Association, 1979.
[29] E. Storm, H. Israel, Report LA-3753 Los Alamos Scientific Laboratory of the University of California, 1967.
[30] J.C. Dainty, R. Shaw, Image Science, Academic Press, London, 1974.
[31] J. Sandrik, R.F. Wagner, Appl. Opt. 20 (1981) 2795.
[32] R.K. Swank, J. Appl. Phys. 44 (1973) 4199.
[33] J.R. Greening, Fundamentals of Radiation Dosimetry, 2nd Edition, IOP, Bristol, UK, 1992, pp. 6–34.
[34] I. Kandarakis, et al., Appl. Phys. A 67 (1998) 521.
[35] D. McLean, Med. Phys. 26 (1999) 643.
[36] A. Papoulis, Probability Random Variables and Stochastic Processes, McGraw-Hill, New York, 1965.
[37] E. Kreyszig, Introductory Mathematical Statistics, Wiley, New York, 1970.
[38] J. Lindstrom, G.A. Carlsson, Phys. Med. Biol. 44 (1999) 1353.
[39] C.J. Vyborny, C.E. Metz, K. Doi, Radiology 136 (1980) 465.
[40] H.W. Venema, Radiology 130 (1979) 765.
[41] J. Beutel, E.L. Kitts, Proc SPIE 2708 (1996) 233.
[42] I. Cunningham, in: J. Beutel, H. Kundel, R. Van Meter, Handbook of Medical Imaging, Vol. 1, SPIE Press, 2000 (Chapter 2).